Conformational Selection During Weak Binding at the Actin and Myosin Interface

Jin Xu and Douglas D. Root[1]
Department of Biological Sciences, University of North Texas, Denton, Texas 76203-5220 USA

ABSTRACT The molecular mechanism of the powerstroke in muscle is examined by resonance energy transfer techniques. Recent models suggesting a pre-cocking of the myosin head involving an enormous rotation between the lever arm and the catalytic domain were tested by measuring separation distances among myosin subfragment-2, the nucleotide site, and the regulatory light chain in the presence of nucleotide transition state analogs. Only small changes (<0.5 nm) were detected that are consistent with internal conformational changes of the myosin molecule, but not with extreme differences in the average lever arm position suggested by some atomic models. These results were confirmed by stopped-flow resonance energy transfer measurements during single ATP turnovers on myosin. To examine the participation of actin in the powerstroke process, resonance energy transfer between the regulatory light chain on myosin subfragment-1 and the C-terminus of actin was measured in the presence of nucleotide transition state analogs. The efficiency of energy transfer was much greater in the presence of ADP-AlF_4, ADP-BeF_x, and ADP-vanadate than in the presence of ADP or no nucleotide. These data detect profound differences in the conformations of the weakly and strongly attached cross-bridges that appear to result from a conformational selection that occurs during the weak binding of the myosin head to actin.

INTRODUCTION

Recent advances in the biophysical studies of force generation in muscle have confirmed many previous theories of muscle contraction and posed important questions about the molecular mechanisms of the powerstroke. In vitro assays of purified actin sliding over myosin have demonstrated that only two types of proteins are required to produce filament sliding over myosin in an ATP-dependent manner (Kron et al., 1991; Finer et al., 1994). X-ray crystallography has provided detailed maps of the relative locations of the critical structures on actin and myosin (Kabsch et al., 1990; Rayment et al., 1993). Chemical modification and cross-linking studies have identified essential communication junctions between the nucleotide-binding site and actomyosin binding (Burke and Reisler, 1977; Wells and Yount, 1979; Burghardt et al., 1997). Spectroscopic studies support the participation of a swinging cross-bridge in force generation by detecting a distinct rotation of probes on the RLC during active muscle contraction (Allen et al., 1996; Baker et al., 1998). Electron microscopy studies provide pictures of a variety of interactions of myosin heads on actin (Craig et al., 1985; Applegate and Flicker, 1987; Pollard et al., 1993). Resonance energy transfer studies have detected nucleotide-dependent motions of varying sizes between a variety of sites (Smyczynski and Kasprzak, 1997; Xu and Root, 1998; Xiao et al., 1998).

Fundamental questions that must still be addressed include 1) what is the precise size of the powerstroke? 2) what are the conformational changes causing force generation? and 3) what is the extent of actin's role in force generation? A variety of experimental methods have been used to try to address the first question, including studies on single molecules and in muscle fibers. Direct measurements of single molecules have produced data with a variety of interpretations ranging from 5 to 17 nm for a powerstroke (Finer et al., 1994; Ishijima et al., 1994). Fiber studies report larger interaction distances of 10–30 nm per ATP (Huxley and Simmons, 1971; Higuchi and Goldman, 1991). The length of the myosin head is 15–20 nm, so a rotation of the entire head might encompass this reported range of powerstroke sizes. Interdomain motions between the catalytic and light chain-binding domains of the myosin head in the absence of ATP have been demonstrated by EPR (Adhikari et al., 1997), electron microscopy (Whittaker et al., 1995), and at high resolution by x-ray crystallography (Dominguez et al., 1998; Houdusse et al., 1999). Interdomain motion might be consistent with a powerstroke length of ~15 nm. Unfortunately, the potential for large and flexible motion does not necessarily guarantee that such conformational changes produce force.

Considerable evidence now exists for variations in the interactions of the myosin head with actin as well as different possible orientations of the light chain domain relative to the catalytic domain. Electron microscopy studies have

Received for publication 3 December 1999 and in final form 27 April 2000.

Address reprint requests to Dr. Douglas D. Root, Dept. of Biological Sciences, Science Research Building, University of North Texas, P.O. Box 305220, Denton, TX 76203-5220. Tel.: 940-565-2683; Fax: 940-565-4136. E-mail: droot@unt.edu.

Abbreviations used: RLC, regulatory light chain; AlF_4^-, aluminum fluoride; BeF_x, beryllium fluoride; CY3, trademark name; CY5.5, trademark name; DTPA, diethylenetriaminepentaacetic acid; *E*, efficiency of resonance energy transfer; ELC, myosin essential light chain; EPR, electron paramagnetic resonance; FITC, fluorescein isothiocyanate; HMM, heavy meromyosin; *J*, overlap integral; κ^2, orientation factor; LMM, light meromyosin; η, refractive index; Φ_D, quantum yield of the donor; *R*, Förster separation distance; R_o, critical transfer distance; RET, resonance energy transfer; S1, myosin subfragment-1; S2: myosin subfragment-2; τ_d, lifetime of the donor in the absence of the acceptor; τ_{da}, sensitized emission lifetime of the acceptor in the presence of the donor; TRITC, tetramethylrhodamine isothiocyanate.

0006-3495/00/09/1498/13 $2.00

observed many orientations of individual myosin heads on actin both in vitro and in muscle (Pollard et al., 1993). Chemical cross-linking studies have identified at least two rigor interactions of myosin with actin (Andreeva et al., 1993). EPR studies have uncovered disordered to ordered transitions of myosin head interactions with actin (Thomas et al., 1995). The swinging lever arm hypothesis postulates that the myosin head enters a pre-cocked state upon hydrolyzing ATP to ADP-Pi but before binding to actin and that the transition to the pre-cocked state changes the position of the light chain-binding domain relative to the catalytic domain in a direction opposite to and equal in magnitude to that which occurs during the powerstroke when myosin is bound to actin. Although much evidence exists that conformational changes in myosin occur during this part of the ATPase cycle, it is far from clear that these detected conformational changes are of sufficient magnitude to confirm lever arm movements of the size suggested using atomic models or measured by interaction distances (Higuchi and Goldman, 1991; Goldman, 1998; Houdusse et al., 1999).

Following our previous work (Xu and Root, 1998) we have used resonance energy transfer techniques to look for changes in the average position of the light chain-binding domain relative to myosin S2, the catalytic domain, and Cys-374 on actin in the presence and absence of nucleotide analogs. These results indicate that if large powerstrokes (>10 nm) are driven by a lever arm mechanism, a pre-cocking of the lever arm must occur during the binding of myosin to actin.

MATERIALS AND METHODS

Proteins and reagents

Papain, maleimide, DTNB, ATP, sodium orthovanadate, beryllium, aluminum chloride, sodium fluoride, and DTPA were procured (Sigma, St. Louis, MO). Cytosine was purchased from Aldrich (Milwaukee, WI). Luminescent chemicals included CY3 (Amersham Life Science, Inc., Arlington Heights, IL), terbium chloride hexahydrate (Aldrich) and FITC (Sigma). CY3-maleimide was prepared as previously described (Xu and Root, 1998). Monoclonal antibodies to myosin S2 (MF30) and to LMM (MF20) (Bader et al., 1982) were obtained from the Developmental Studies Hybridoma Bank and purified by Sephadex G-75 FPLC. The Fab was prepared by papain digestion and purified by DEAE-Sepharose ion-exchange chromatography. Rabbit skeletal actin was prepared by the method of Spudich and Watt (1971) and stored in G-buffer. Free nucleotides were removed immediately before use by dialysis for 6–8 h in the assay buffer. Rabbit skeletal myosin was prepared by the method of Godfrey and Harrington (1970). S1 was obtained from myosin with papain digestion and separated according to the methods of Weeds and Pope (1977). The protein concentrations were determined using extinction coefficients at 280 nm of 0.55 $(mg/ml)^{-1}$ cm^{-1}, 0.60 $(mg/ml)^{-1}$ cm^{-1}, and 0.75 $(mg/ml)^{-1}$ cm^{-1} for myosin, RLC, and S1, respectively, and at 290 nm of 0.63 $(mg/ml)^{-1}$ cm^{-1} for actin.

Acto-S1 affinity assay in the presence of different nucleotide analogs

Actin was labeled with pyrene-iodoacetamide according to Cooper et al. (1983). Labeling ratios ranged from 0.64 to 1.0 pyrenes per actin for different preparations. The fluorescence was detected at 410 nm with the excitation at 377 nm. The fluorescence was quenched when S1 molecules associated with the labeled F-actin. Equimolar S1 and actin (1 μM) were used in the experiments. After a small amount of ATP (5 μM) was hydrolyzed by myosin to ADP, phosphate analogs were added (AlF_4 0.1 mM, BeF_x 0.1 mM, vanadate 0.2 mM, and vanadate 1 mM). The maximal increase of fluorescence caused by S1 dissociation in the presence of nucleotide analogs was compared to the difference between the intensities with S1 bound and with S1 dissociated by ATP, which yielded the ratios of acto-S1 dissociation. Apparent rates of dissociation were estimated by fitting the time trace curves to an exponential function.

In vitro motility assays

In vitro motility assays of actin sliding over myosin on a dimethyldichlorosilane-coated coverslip were performed in 4 mM $MgCl_2$; 25 mM KCl; 1 mM EGTA; 10 mM DTT; 25 mM imidazole, pH 7.4; 0.5 mg/ml BSA; and 0.5% methylcellulose (Kron et al., 1991) at 30°C. Actin was labeled with TRITC-phalloidin and imaged with an ICCD 350F (Videoscope Int., Sterling, VA) upon epifluorescence excitation with a helium neon green laser in a Zeiss IM35 inverted microscope equipped with a stage heater to maintain the temperature at 30°C. Images were recorded with an SVHS video recorder (Panasonic) and subsequently captured to NIH Image (version 1.60 by Wayne Rasband) through a Scion framegrabber (Frederick, MD) on a Power Macintosh computer (Apple Computer, Cupertino, CA). The sliding velocities of moving filaments were analyzed by our previously developed Autotrack software (Root and Wang, 1994).

Protein labeling

RLC was dissociated from rabbit skeletal myosin with DTNB and purified by ethanol precipitation and Superdex 75 FPLC (Wagner, 1982; Xu and Root, 1998). The purified RLC was labeled with cytosine-DTPA terbium chelate (Root, 1997). After incubating the myosin or S1 in 0.5 M KCl, 2 mM EDTA, 10 mM imidazole, pH 8.0, for 15 min at room temperature to dissociate the original RLC, the myosin was precipitated by adding 10 volumes of cold water, or the S1 was purified by Superdex 75 gel filtration. Then the labeled RLC was exchanged back to the myosin or S1 in 0.5 M NaCl, 5 mM $MgCl_2$, 10 mM imidazole, pH 7.0. The average labeling ratio of the myosin after exchanging was 20% as determined by terbium titration on seven independent preparations, and no effect on ATPase activity was observed. When the Fab of MF30 was labeled with a cytosine-DTPA terbium chelate to work as the resonance energy transfer donor, the labeling procedure was the same as that for RLC labeling. Before the resonance energy transfer experiments, the labeled Fab was incubated with myosin for 30 min, and 10 volumes of cold water were added to precipitate the myosin. When Fab was labeled with FITC to be the acceptor, the molar ratio of FITC to Fab was 10 during the labeling, and the average labeling ratio was 0.4 mol of FITC incorporated per mol of Fab ranging from 0.32 to 0.5 for different preparations.

F-actin was labeled with CY3-maleimide or tetramethylrhodamine-iodoacetamide. Approximately 10 μM F-actin was reacted with 50 μM of the labeling reagent in 0.1 M KCl, 2 mM $MgCl_2$, 10 mM imidazole, pH 7.0 at 4°C overnight. The average labeling ratios were 20% based on five independent preparations, which were determined by UV-visible absorbances (extinction coefficients of 150,000 M^{-1} cm^{-1} at 552 nm and 12,000 M^{-1} cm^{-1} at 280 nm for CY3; 96,900 M^{-1} cm^{-1} at 556 nm; and 20,150 M^{-1} cm^{-1} at 290 nm for tetramethylrhodamine-5-iodoacetamide). The fluorescence of the actin band decreased with the increasing digestion time with carboxypeptidase A, which confirmed that the labeling site was on Cys-374.

Resonance energy transfer

An SLM-Aminco Bowman II luminescence spectrometer (Spectronic Instruments, Rochester, NY) with dual xenon arc and flashlamp light sources

was used to record the luminescence spectra. Delayed luminescence and lifetime measurements were collected after 200 μs following the excitation pulse of the flashlamp at 248 nm. Delayed emission spectra were accumulated over a gate period of 4 ms. Luminescence decay curves were obtained at a resolution of 100 μs and averaged for 100-1000 repetitions to increase the signal-to-noise ratio. The lifetimes of the decay curves were calculated by MacCurvefit Software (version 1.3.3 by Kevin Rainer).

In this research, the donor of the resonance energy transfer pair was phosphorescent terbium. Although free terbium is weakly luminescent due primarily to its very low absorbance and high degree of quenching by water, its signal and lifetime are enhanced by a chromophore, cytosine, which participates with DTPA in the chelation of terbium and transfers energy to terbium. The emission spectrum of terbium is unique in that it has four sharp peaks in the visible region at 489, 547, 589, and 622 nm, with no emissions between the peaks. These properties are particularly useful for resonance energy transfer coupling to a variety of fluorophores that absorb and emit in the visible spectrum, such as fluorescein and CY3 in this research. To eliminate any errors due to uncertainty in the extent of labeling by donors and acceptors, the efficiency of energy transfer was determined by comparing lifetime measurements of the donor without acceptor present and the sensitized emission of the acceptor in the presence of the donor (Selvin and Hearst, 1994). The sensitized emission of the fluorescent acceptor is only detected if the resonance energy transfer occurs, because a delay is imposed after the pulsed excitation to allow background signals, such as fluorescence, Raman, and other light scattering, to decay to negligible levels before collecting data. The signal from terbium chelate was measured at 547 nm, and the signals of sensitized emission from fluorescein and CY3 were detected at 520 and 568 nm, respectively. The efficiency of RET (E) for the distance (R) between the donor and the acceptor was calculated from the equation:

$$E = 1 - \tau_{da}/\tau_d = \sum_i (R_0^6/R_i^6)/\left(1 + \sum_i (R_0^6/R_i^6)\right) \quad (1)$$

Where τ_{da} is the apparent long-lived lifetime of the acceptor in the presence of the donor, τ_d is the lifetime of the donor in the absence of acceptor, and R_0 is the critical transfer distance. The critical transfer distance was calculated according to the equation:

$$R_0 = (8.79 \times 10^{-11} J \kappa^2 \eta^{-4} \phi_D)^{1/6} \text{nm} \quad (2)$$

Where J is the calculated overlap integrals for the acceptor with terbium, which are 7.6×10^{14} and 5.1×10^{15} for fluorescein and CY3, respectively; κ^2 is the dynamic average value of the orientation factor, 2/3; $\eta = 1.4$; and $\phi_D = \tau_d/4.75$ ms (Root et al., 1999). Uncertainty in the orientation factor will cause at most a 10% error in the separation distance because terbium has an isotropic emission (Selvin and Hearst, 1994).

As the quantum yield of the donor is determined by its radiative lifetime (τ_d), the critical transfer distance (R_0) also depends on the τ_d. These parameters yield $R_0/\phi_D{}^{1/6}$ values of 4.76 and 6.53 nm for fluorescein and CY3 as the acceptors, and ϕ_D varied slightly from one experiment to the next, depending on the τ_d value.

For myosin experiments, the samples were in 0.5 M KCl, 2 mM $MgCl_2$, and 10 mM imidazole, pH 7.0. The acto-S1 experiments were performed in 0.1 M KCl, 2 mM $MgCl_2$, and 10 mM imidazole, pH 7.0. The concentrations of labeled myosin and S1 were 0.5–2.0 μM. When present, the actin concentration was two times the myosin or equal to the S1 concentration, AlF_4 was 0.1 mM, BeF_x was 0.1 mM, and orthovanadate was 0.2 mM. Increasing the S1/actin ratio did not change the resonance energy transfer efficiency (data not shown). Substoichiometric amounts of CY3-ATP were used to avoid diffusion-enhanced energy transfer (Xu and Root, 1998).

RESULTS

The correlations between domain movements in myosin and the adenosine triphosphatase cycle were examined by resonance energy transfer. Probes were attached to myosin S2 via a monoclonal Fab fragment, to the light chain-binding domain by labeling the N-terminus of the RLC, to the catalytic domain using CY3-ATP, or to actin on Cys-374. Transition states were examined using nucleotide analogs or single ATP turnovers in stopped-flow resonance energy transfer measurements. Controls for labeling effects included 1) in vitro motility assays that are exquisitely sensitive to even small fractions of inactivated myosins, none of which was detected upon antibody labeling; 2) a labeled antibody to LMM that did not produce detectable resonance energy transfer, thereby verifying the efficacy of the labeling method; 3) previous characterizations of myosin labeled at the N-terminus of the RLC that have not detected effects on myosin function by either ATPase activity assays or in vitro motility assays (Wolff-Long et al., 1995; Xu and Root, 1998); and 4) previous characterizations of CY3-ATP on myosin ATPase activity or fiber shortening indicating active labeled myosin (Funatsu et al., 1995; Xu and Root, 1998). Clearly, the largest responses to the nucleotide transition state analogs were detected by the changes in the sensitized emission lifetimes of energy transfer between the RLC and Cys-374 on actin, indicating that weak binding to actin plays a critical role in preparing myosin for a subsequent powerstroke.

In vitro motility of antibody-bound myosin

Because there was no specific fluorescent labeling method for the skeletal myosin rod, we established a fixed point on the S2 as a reference for resonance energy transfer by attaching the luminescent probes to the Fab of the monoclonal antibody, MF30. To determine whether myosin's function was impeded by the binding of MF30 to myosin S2, in vitro motility assays were performed in the presence and absence of the antibody. As shown in Fig. 1, the distribution pattern of sliding velocity is similar for myosin with and without antibody. The average sliding velocity of the control in the absence of antibody was 4.71 $\pm$ 0.24 μm/s. Compared with the velocity in the presence of MF30 antibody (4.64 $\pm$ 0.23 μm/s), there was a slight decrease, which was not statistically significant. The results of in vitro motility assays showed that the myosin molecules functioned normally with antibody bound to the S2.

Resonance energy transfer from RLC to Fab on the myosin rod and from Fab to the nucleotide site

The resonance energy transfer between the RLC and the S2 was achieved by labeling the N-terminal region of the RLC with the resonance energy transfer donor, a terbium chelate, and the Fab of MF30 with the acceptor, FITC. When the Fab was bound to the rod, the donor quenching and the

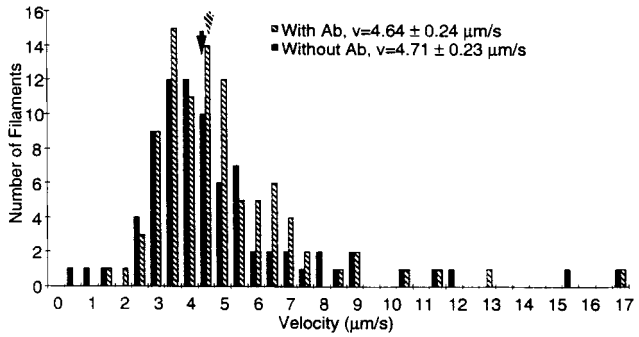

FIGURE 1 Functionality of labeled myosin demonstrated by in vitro motility assays of actin sliding over myosin with and without MF30. The actin was labeled with tetramethyl rhodamine phalloidin and the assays were performed in 4 mM $MgCl_2$; 25 mM KCl; 1 mM EGTA; 10 mM DTT; 25 mM imidazole, pH 7.4; 0.5 mg/ml BSA; and 0.5% methylcellulose at 30°C. Velocity distribution histograms of actin sliding over myosin with and without antibody bound are shown with shaded bars and solid bars. The molar ratio of MF30 to myosin is 2.5. The distribution pattern of sliding velocity and average velocity for myosin bound by MF30 is very similar to those for free myosin. This shows that the binding of the antibody to myosin did not change its normal function.

sensitized emission at 520 nm showed significant resonance energy transfer between the probes (Fig. 2 *A*). Because the molar ratio of myosin to Fab was 2:1, and the average labeling ratio for Fab was 40%, the resonance energy transfer was thought to occur through a single separation distance, which was supported by the observation that a single exponential fits the sensitized emission lifetime data. As a control that the antibody labeling was specific, a similar monoclonal antibody, MF20, but against LMM rather than S2, was used to label the myosin rod. Unlike the MF30, the MF20 did not produce detectable resonance energy transfer, because the LMM is located too far from the RLC. The lifetime measurements for labeled myosin with and without MF30 Fab are illustrated in Fig. 2 *A1*. The lifetime for the terbium chelate labeled S1 alone was 1.62 ms, and upon binding the fluorescein-Fab of MF30, the lifetime decreased to 1.12 ms (Table 1). The distance separation in the no nucleotide state was almost identical to that for the ADP state. The addition of F-actin did not significantly change the measured efficiency of resonance energy transfer. In the presence of different nucleotide analogs (ADP-AlF_4, ADP-BeF_x, ADP-vanadate), the efficiency of resonance energy transfer increased slightly compared with the rigor state. However, the magnitude of the calculated change in separation distance was far smaller than the size of the displacement by a myosin powerstroke.

There were only small distance changes between the nucleotide site and the RLC or between the RLC and S2 for different nucleotide analogs. To complete a triangle, resonance energy transfer was measured from the donor (terbium chelate) on the Fab to the acceptor (CY3-ADP) in the nucleotide pocket, which extended the detection range over catalytic domain, neck region, S2, and the junction between them. Donor quenching at 547 nm and sensitized emission at 568 nm (Fig. 2 *B*) confirmed the occurrence of resonance energy transfer. The decay curves for the donor alone and the donor with acceptor are illustrated in Fig. 2 *B1*. Upon adding the different phosphate analogs (AlF_4, BeF_x, vanadate), the lifetime of the donor with acceptor (τ_{da}) demonstrated little change (Table 2). These data indicate that there is little change in distance between the catalytic domain and S2 in the presence of different nucleotide analogs. The nucleotide analogs induce slight decreases by ~0.1–0.3 nm in the separations between the RLC and either the S2 or the nucleotide site. If these differences are real, they suggest that the N-terminus of the RLC might change its average position when the transition state nucleotide analogs are added.

Emission intensity in stopped-flow experiments

To confirm the resonance energy transfer results, three stopped-flow experiments were performed in this research: 1) labeled myosin (terbium chelate on RLC) with CY3-ATP, 2) bi-labeled myosin (terbium chelate on RLC and fluorescein on Fab) with ATP, and 3) terbium chelate labeled Fab-conjugated myosin and CY3-ATP. Because the resonance energy transfer was occurring between the coupled donor and acceptor (terbium and CY3, or terbium and fluorescein), the interdomain movements during ATP hydrolysis could be monitored by the fluorescence intensity of the donor or the acceptor. Upon mixing the labeled myosin (chelated-terbium on the RLC) and CY3-ATP, the emission intensity at 568 nm demonstrated a slight decrease during the first 25 s (Fig. 3 *A*). The plot of the first 500 ms (Fig. 3 *A1*) confirmed that the emission intensity did not show a large change with 10-ms resolution data. The results for stopped-flow experiments of bi-labeled myosin (chelated-terbium on the RLC and fluorescein-Fab on the rod) are shown in Fig. 3 *B* (for 25 s) and Fig. 3 *B1* (for 500 ms). There was similarly no notable variation in the signal from terbium chelate labeled Fab-conjugated myosin and CY3-ATP (Fig. 3, *C* and *C1*) as the luminescence intensity remained constant for 25 s. Because the stopped-flow experiments monitor the conformational changes during ATP hydrolysis without the need for nucleotide analogs, the results of the stopped-flow experiments demonstrated a further restriction on the magnitude of interdomain movements within the myosin molecule that occur in the absence of actin.

Binding affinity of S1 to F-actin in the presence of different nucleotide analogs

The presence of different nucleotide analogs in the active site of S1 decreases the binding constant of S1 to actin (Phan et al., 1993; Werber et al., 1997). To investigate the structural transitions in the interface of actomyosin during

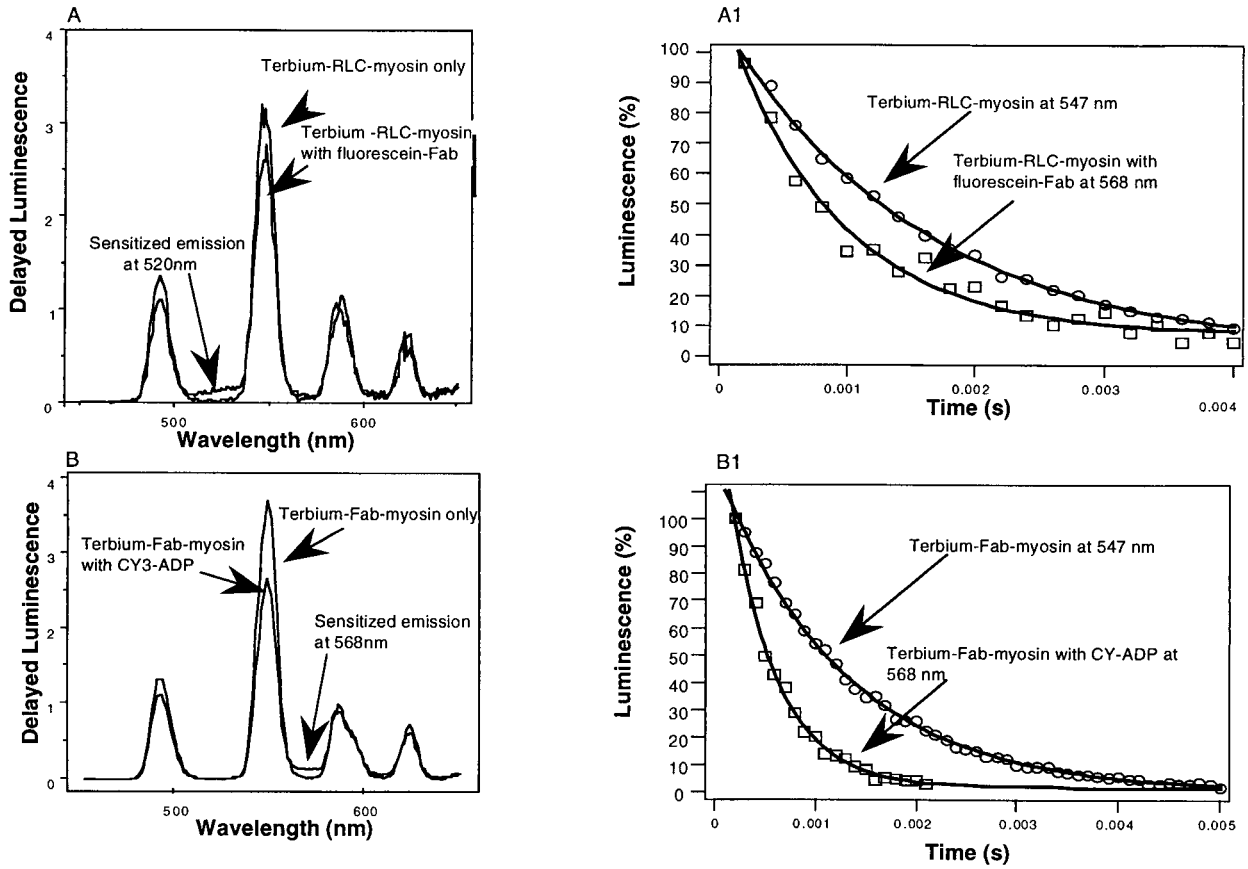

FIGURE 2 Absence of myosin pre-cocking detected in delayed emission spectra and decay curves of terbium-RLC-myosin with and without fluorescein-Fab to myosin S2 (*A*, *A1*) and terbium-Fab-myosin with and without CY3-ADP (*B*, *B1*). The spectra were collected in an SLM-Amico Bowman II luminescence spectrometer with excitation of a flashlamp at 248 nm followed by a 200-μs delay before collecting readings for 4 ms. The bandpass of emission is 4 nm. The energy transfer donor terbium chelate on the RLC (*A*) and on the Fab of a monoclonal antibody to the rod (*B*) showed four sharp peaks at 490, 547, 590, and 623 nm without emissions between them. Upon adding the acceptors, fluorescein-labeled Fab (*A*) and CY3-ADP (*B*), the sensitized emission at 520 nm (*A*) and 568 nm (*B*) and the donor quenching at 547 nm demonstrated that the resonance energy transfer was occurring. The decay curves (*A1*, *B1*) were obtained after excitation at 248 nm followed by a 200-μs delay with a resolution of 200 μs and averaged for 300 repetitions. Because the acceptor CY3 is not phosphorescent, the lifetime of the sensitized emission at 568 nm is equal to the lifetime of the donor in the presence of the acceptor.

ATP hydrolysis with the nucleotide analogs, the amount of S1 that still formed acto-S1 complex in the presence of the different nucleotide analogs was determined first. The quenching of pyrene-actin during the binding of S1 to actin was measured upon binding ADP followed by AlF_4, BeF_x, and vanadate, respectively. The fluorescence of pyrene-actin was quenched when the acto-S1 complex formed, and the effects of phosphate analogs with ADP on acto-S1 were determined from the fluorescence dequenching upon S1 dissociation. Fig. 4 shows the dissociation ratios calculated from the dequenching and the apparent dissociation rates

TABLE 1 The parameters of resonance energy transfer between myosin RLC and Fab on S2 for rigor and different nucleotide analog states

Samples	τ_d (ms)	τ_{da} (ms)	E	R (nm)
No nucleotide	1.62 ± 0.08	1.12 ± 0.08	0.31 ± 0.01	4.6 ± 0.1
ADP	1.64 ± 0.06	1.09 ± 0.14	0.34 ± 0.06	4.5 ± 0.2
ADP · Actin	1.68 ± 0.01	1.08 ± 0.22	0.34 ± 0.09	4.5 ± 0.3
ADP · AlF_4	1.72 ± 0.05	1.09 ± 0.01	0.36 ± 0.02	4.6 ± 0.1
ADP · BeF_x	1.70 ± 0.02	1.01 ± 0.09	0.41 ± 0.05	4.3 ± 0.2
ADP · Vanadate	1.64 ± 0.06	0.99 ± 0.04	0.40 ± 0.01	4.3 ± 0.1

The ± values represent the range from two independent experiments for independent preparations.

TABLE 2 The parameters of resonance energy transfer between Fab on myosin S2 and nucleotide site in the presence of different nucleotide analogs

Samples	τ_d (ms)	τ_{da} (ms)	E	R (nm)
CY3-ADP	1.25 ± 0.01	0.92 ± 0.01	0.27 ± 0.01	6.2 ± 0.1
CY3-ADP · AlF_4	1.25 ± 0.01	0.92 ± 0.04	0.26 ± 0.02	6.2 ± 0.1
CY3-ADP · BeF_x	1.25 ± 0.01	0.88 ± 0.02	0.29 ± 0.01	6.1 ± 0.1
CY3-ADP · Vanadate	1.25 ± 0.01	0.90 ± 0.07	0.28 ± 0.05	6.1 ± 0.2
CY3-ADP · Actin	1.24 ± 0.01	0.90 ± 0.04	0.28 ± 0.02	6.1 ± 0.1

The ± values represent the range from two independent experiments for independent preparations.

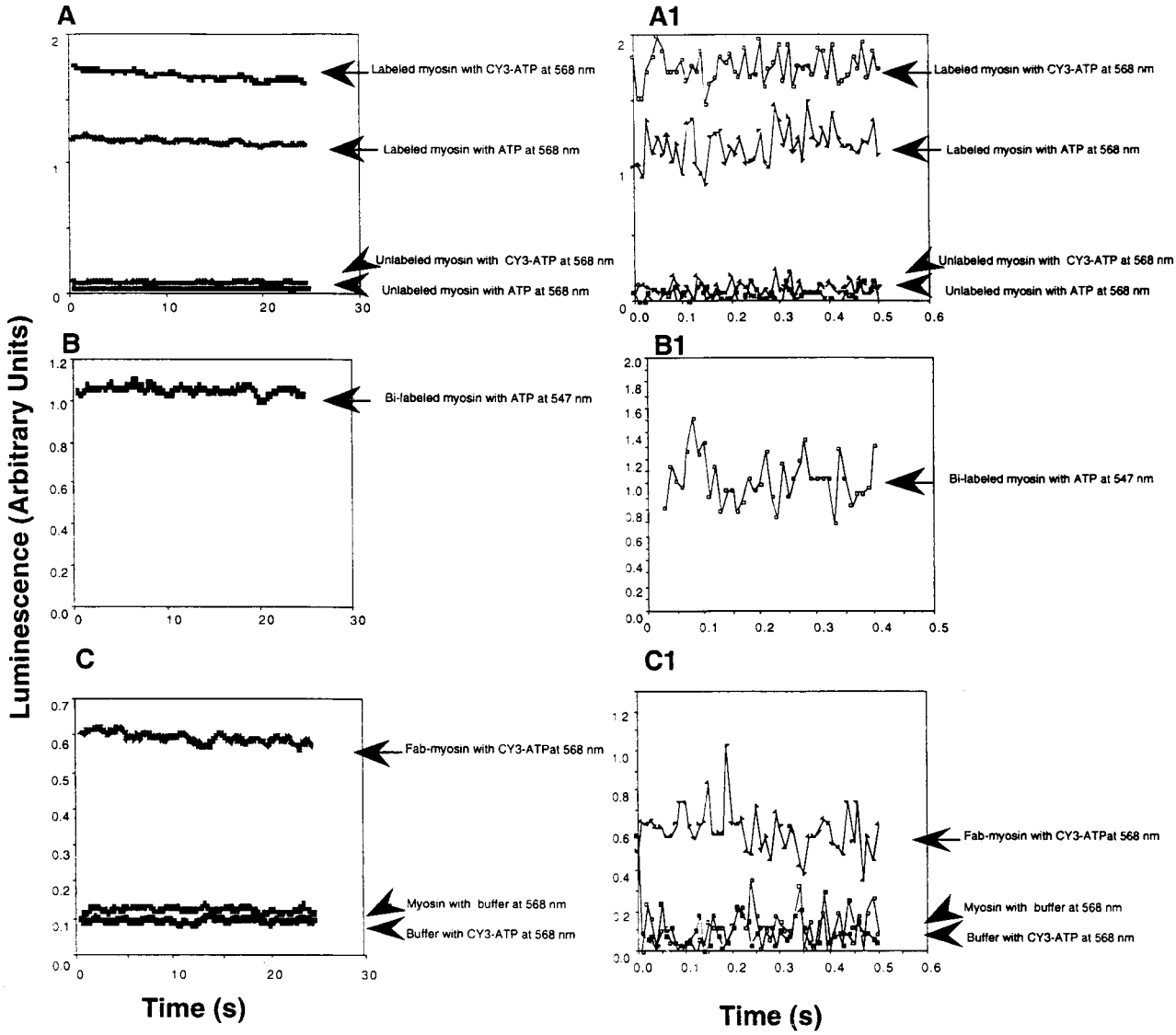

FIGURE 3 Absence of myosin pre-cocking shown by emission intensity in stopped-flow experiments. The emission intensity was recorded from 0 to 25 s after flashlamp excitation at 248 nm with a resolution of 10 ms. Upon mixing the exchanged myosin (chelated-terbium on the RLC) (*A*) and antibody-conjugated myosin (*C*) with CY3-ATP, the emission intensity at 568 nm remained constant for 25 s. The zoomed-in picture for the first 500 ms (*A1* and *C1*) more clearly showed that the emission intensity did not change significantly. The results for stopped-flow experiments of bi-labeled myosin (chelated-terbium on the RLC and fluorescein-Fab on the rod) were shown in *B* (for 25 s) and *B1* (for 500 ms). There is still no significant variation for the emission intensity of the donor at 547 nm and the acceptor at 520 nm.

estimated by fitting the data to an exponential function. Upon binding ADP with the phosphate analogs, >50% of S1 dissociated from the actin filament, and the highest dissociation extent was for AlF_4. The results are consistent with cosedimentation and kinetic studies (Phan et al., 1993; Werber et al., 1997).

Resonance energy transfer between actin Cys-374 and the RLC of S1

In our previous research, the resonance energy transfer between the RLC and the nucleotide did not show any significant distance change during ATP hydrolysis (Xu and Root, 1998). The distances between the RLC and S2 and also between the nucleotide site and S2 were detected in this research by using a monoclonal antibody against S2 to establish a fixed point for resonance energy transfer, and the changes remained insignificant in the presence of different nucleotide analogs. The lack of energy transfer changes in response to nucleotide analog binding within the myosin molecule alone influenced us to examine the effects of actomyosin interaction. In order to search for a structural transition involving the actomyosin interface, a unique maleimide version of the CY3 was attached to actin Cys-374 to

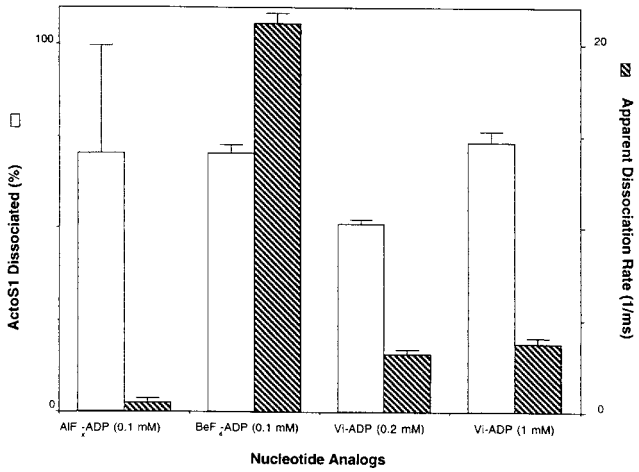

FIGURE 4 Phosphate analogs mimic weak binding states of S1. Fluorescence dequenching of pyrene-labeled actin upon S1 dissociation was used to assess the effects of phosphate analogs with ADP on acto-S1 dissociation. Just as in the resonance energy transfer measurements, S1 (1 μM) was added to F-actin (1 μM) and small amounts of ATP (5 μM). After the ATP hydrolyzed to ADP, phosphate analogs were added as indicated in the histogram. The maximal increase in fluorescence quenching was compared to the difference between the fluorescence intensities of the pyrene actin with S1 bound and with S1 dissociated by ATP to obtain the percentage of dissociation. Apparent rates of dissociation were estimated by fitting the decay curves to an exponential function.

be the acceptor, and the RLC was labeled with terbium chelate and exchanged back to papain S1 as the donor. The resonance energy transfer was occurring between the probes, which was shown by both donor quenching and sensitized emission (Fig. 5 *A*). The decay curves of the exchanged S1 with unlabeled actin and labeled actin in the rigor and different nucleotide states are illustrated in Fig. 5, *B–F*. When different nucleotide analogs were present, the lifetime of the donor (τ_d) with unlabeled actin increased (Table 3). The highest increase was for AlF_4 (from 1.19 ms of the rigor state to 1.49 ms). Such a large change might reflect the conformational or environmental variation of the RLC caused by both the phosphate analogs and actin binding that supports the conformational selection hypothesis, because little change was observed in the absence of actin (Table 1). Both the increase of τ_d and the decrease of τ_{da} lead to a significant augmentation of the resonance energy transfer efficiency. Considering the labeling ratio of actin and S1, the resonance energy transfer could not be occurring in a one-donor to one-acceptor mode. However, when the S1 molecules attached to the actin filament, a certain resonance energy transfer pattern was established. After adding the nucleotide analogs, the S1 randomly detached from the F-actin. Therefore, the efficiency increase must reflect the conformational transition upon actin binding during the myosin ATP hydrolysis cycle.

DISCUSSION

Hypotheses describing the mechanism of force generation by molecular motors can be divided into two categories: those that view a motor acting on a passive scaffold, and those that describe a dynamic and cooperative process between two actively participating molecules. The model proposed by Huxley and Simmons (1971) depicts the myosin head rotating between different angles of attachment at the actomyosin interface in which the angle of the cross-bridge is determined *during* actin binding, suggesting a participation of actin in the powerstroke. In contrast, recent proposals of a swinging lever-arm hypothesis have become popular, in which the bulk of the cross-bridge is envisioned to bind to actin with a more or less fixed geometry and generate force only by internal myosin movements of a light chain-binding domain that pre-cocks *before* actin binding (Rayment et al., 1993; Holmes, 1997; Goldman, 1998). This model is consistent with biochemical and biophysical evidence: variation of the length of the lever arm by genetic engineering can change the speed of transport (Uyeda et al., 1996), electron spin-resonance spectra resolve several coexisting orientations in fibers incorporating a spin-labeled RLC (Baker et al., 1998), and spectroscopic probes on the RLC demonstrate changes in their orientation during isometric contraction (Allen et al., 1996). However, these data can be interpreted alternatively by a myosin head rotation at the actomyosin interface and other models that invoke a more active participation of actin. The present work examines two critical distinctions between models of the powerstroke: 1) the location of the fulcrum(s) for force generation, and 2) the timing of the pre-cocking event(s).

Considering both actin and myosin, ~15–20 nm^2 of protein surface is involved in the rigor state formation (Cooke, 1997). The actomyosin interface is relatively close to the nucleotide site in the structure of myosin, and it is so facile to imagine that the energy released from ATP hydrolysis leads to a certain type of structural transition in the interface, which contributes to the powerstroke. During the ATP hydrolysis cycle, myosin binds to actin in weak and strong binding states whose interconversion is driven by the reduction of electrostatic repulsions between negatively charged phosphate groups upon the release of inorganic phosphate from myosin. Electron microscopy and x-ray diffraction have shown that the cross-bridges adopt disordered orientations in the weak binding state and ordered orientation in the strong binding state (Huxley and Faruqi, 1983; Piazzesi et al., 1999). The powerstroke is thought to be caused by the disorder-to-order transition (Huxley and Kress, 1985; Berger and Thomas, 1993). If the powerstroke involves this transition, there should be a significant conformational change in the actomyosin interface during the ATP hydrolysis cycle.

An atomic-scale ruler can be used to measure conformational changes during the ATP hydrolysis cycle. Resonance

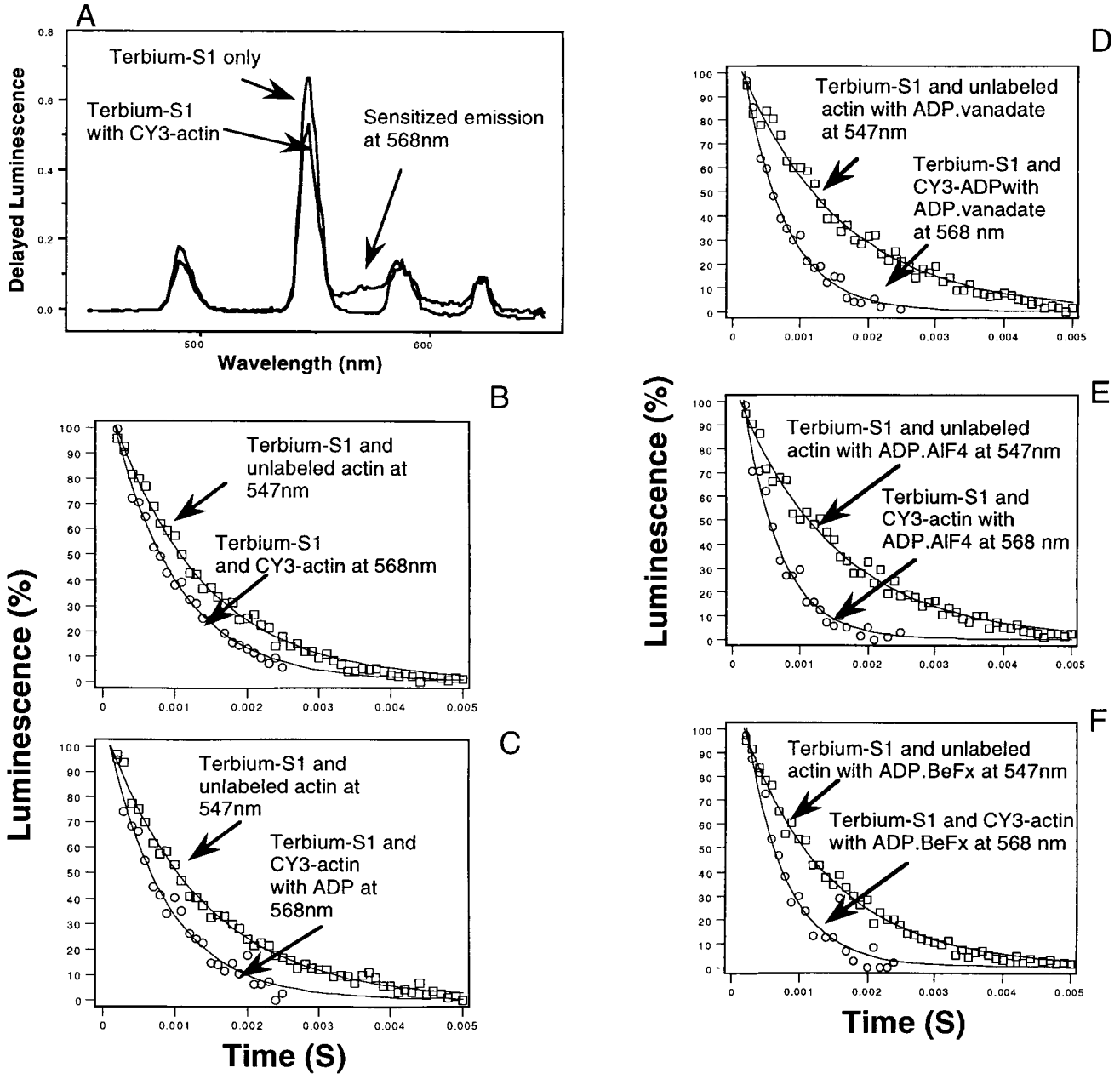

FIGURE 5 Evidence for conformational selection during weak binding to actin in delayed emission spectra of labeled S1 (terbium chelate on the RLC) with and without labeled actin (CY3 on Cys-374) and decay curves with different nucleotide analogs. With the acceptor-labeled F-actin binding to the donor-labeled papain S1, the sensitized emission at 568 nm and the donor quenching at 547 nm demonstrated that the resonance energy transfer was occurring between S1 RLC and actin Cys-374. The decay curves (*B–F*) were collected after flashlamp excitation at 248 nm with a resolution of 200 μs and averaged for 400 repetitions. When ADP · AlF_4 (*D*) or ADP · BeF_x (*E*) were present, the lifetime of the donor only and the sensitized emission changed in comparison with the rigor state (*B*) and ADP state (*C*), which produced a large alteration in the energy transfer efficiency.

energy transfer is a spectroscopic measurement that is sensitive to the average distance between donor and acceptor probes. The distances between the catalytic and light chain domains detected by luminescence resonance energy transfer are consistent with the atomic model of skeletal S1 (Xu and Root, 1998; Xiao et al., 1998; Getz et al., 1998. Table 4). The high sensitivity and accuracy of luminescence resonance energy transfer make it feasible to test the conformational changes in actomyosin during the powerstroke by attaching the probes on actin and myosin molecules. In our previous research, no significant interdomain movement was detected between the N-terminal region of the RLC and nucleotide site using the ADP, ADP-vanadate, ADP-AlF_4, and ADP-BeF_x nucleotide analogs (Xu and Root, 1998). In

TABLE 3 The parameters of resonance energy transfer between myosin S1 RLC and actin CYS374 for rigor and different nucleotide analog states

Samples	$\tau_d \pm$ SD (ms)	$\tau_{da} \pm$ SD (ms)	$E \pm$ SD (%)
Rigor	1.19 ± 0.23	0.74 ± 0.15	0.38 ± 0.03
ADP	1.23 ± 0.27	0.77 ± 0.17	0.37 ± 0.03
ADP · AlF_4	1.49 ± 0.17	0.57 ± 0.10	0.63 ± 0.06
ADP · BeF_x	1.48 ± 0.17	0.51 ± 0.07	0.66 ± 0.05
ADP · Vanadate	1.23 ± 0.26	0.60 ± 0.17	0.52 ± 0.09

The data are from four independent experiments for independent preparations.

this research, the probes were attached to a monoclonal antibody to myosin S2 (MF30), and the distances were measured from the Fab to RLC and to the nucleotide site in the presence of different nucleotide analogs and actin. Because there were still no large changes detected, the filament sliding in skeletal myosin might not be caused simply by large conformational changes in the myosin molecule itself, and the actomyosin interface is likely to play a role in the process. By labeling actin Cys-374 with the CY3 acceptor and myosin RLC with the terbium chelate donor, large differences in the efficiency of resonance energy transfer were detected using nucleotide analogs. These observations suggest that there is a considerable conformational alteration in the actomyosin interface, which might contribute to the force generation and the powerstroke.

Correlations with x-ray crystallographic structures

Recent crystallographic structures have clearly defined different orientations in the position of the lever arm relative to the catalytic domain of myosins from skeletal muscle, smooth muscle, *Dictyostelium*, and scallop (Rayment et al., 1993; Fisher et al., 1995; Dominguez et al., 1998; Houdusse et al., 1999). These structures have been grouped into three different classes (Houdusse et al., 1999): state I (similar to skeletal with no nucleotide), state II (similar to smooth with AlF_4-ADP), and state III (similar to scallop with ADP). If one compares the distances separating homologous amino acid residues in these atomic models it becomes apparent that striking differences between states I and III are not reflected by the range of RET distance determinations with a variety of nucleotide analogs, indicating that not all the states are individually represented in the RET measurements (Table 4). For the majority of RET measurements, state I is the most consistent; however, it is interesting to note that the lever arm position in state I is intermediate between its positions in states II and III. It is not difficult to imagine that some combination of states I–III exists simultaneously in solution at any given point in time, yielding an average structure most similar to state I. Although evidence of some conformational change induced by nucleotide transition state analogs is apparent in RET measurements of myosin alone in solution, the magnitudes of the average differences are not as striking as those stabilized in crystals.

Although it has been suggested that these structures represent different stages of the powerstroke, the correlations between the powerstroke stages and the form of the bound nucleotide in the crystallographic structure are weak. When ADP is bound to the nucleotide site, completely different conformations of the catalytic domain in *Dictyostelium* (state I) and scallop (state III) are crystallized. When ADP-BeF_x is bound, the smooth muscle myosin crystal structure (state II) is very different from those found in *Dictyostelium* and scallop (both state I). In contrast, ADP-AlF_4 presents similar structures in smooth (state II) and *Dictyostelium* (state II), and ADP-vanadate presents similar structures in scallop (state II) and *Dictyostelium* (state II). Myosins with no nucleotide bound crystallized in state I for skeletal and scallop. The matrix correlation of the three-state model with the nucleotide bound is not statistically significant ($r^2 = 0.195$, $p > 0.2$), which suggests that factors other than the bound nucleotide are predominantly determining the lever arm position in the crystal structure. Such factors may include the source of the myosin, crystal packing forces, and crystallization conditions. Similarly, cryoelectron micrograph reconstructions of actin decorated with brush-border myosin (Jontes and Milligan, 1997) or with smooth muscle myosin (Whittaker et al., 1995) show substantial rotations of the lever arm to varying degrees away from rigor upon binding ADP. These observations also do not correlate with evidence indicating that phosphate release is directly coupled to the powerstroke. To reconcile such inconsistencies, suggestions have been made that certain structures with one type of nucleotide bound might actually represent a different nucleotide transition state, such as the ADP-scallop myosin structure representing the ATP-bound state.

Thermodynamic considerations and a role for conformational selection

The lever arm theory postulates that the form of the nucleotide bound dictates a unique conformation of the myosin that drives a force generating movement of the lever arm. Although ATP supplies the energy for the powerstroke (although that energy may be stored temporarily in other structures), the free energy of ATP hydrolysis and phosphate dissociation should determine the equilibrium position of a lever arm during the powerstroke. Several transitions exist during the ATP hydrolysis cycle that may be associated with different free energy levels (Lymn and Taylor, 1971): ATP binding, actomyosin dissociation, ATP hydrolysis to ADP-Pi, weak actin binding, phosphate release, strong actin binding, and ADP release. Two of these transitions, the weak binding of ADP-Pi S1 to actin and ADP release, are not favored thermodynamically, but the cycle is driven by the strong negative ΔG° of the other

TABLE 4 Crystallography and RET between the catalytic and light-chain domains

Residues (skeletal equivalents)*	State I Skeletal	State II Smooth	State III Scallop	RET Distances (for various states)
ADP-N-terminus (RLC)				6.9 nm –6.2 nm[†]
W131-G21 (ELC)[‡]	6.6 nm	5.1 nm	9.3 nm	
W131-V103 (RLC)	5.8 nm		9.2 nm	6.6 nm–6.0 nm[§]
N127-C177 (ELC)	3.9 nm	4.3 nm	5.0 nm	4.9 nm–5.5 nm[¶]
K83-C177 (ELC)	2.4 nm	4.7 nm	3.2 nm	2.5 nm–2.6 nm[¶]
K553-C177 (ELC)	7.5 nm	6.3 nm	7.2 nm	4.8 nm–5.3 nm[¶]

*Sequence alignments with identities underlined:

HC	K83
Skeletal	M N P P K Y D K I E D M A
Smooth	M N P P K F S K V E D M A
Scallop	M N P P K F E K L E D M A

HC	N127 W131
Skeletal	L F C V T V N P Y K W L P
Smooth	L F C V V I N P Y K Q L P
Scallop	L F C I A V N P Y R R L P

HC	K553
Skeletal	F P K A T D T S F K N K L
Smooth	F P K A T D T S F V E K L
Scallop	F P K A D D K S F Q D K L

ELC	G21
Skeletal	F L L F D R T G D A K
Smooth	F Q L F D R T G D G K
Scallop	F E L F D F W D G R D G A

ELC	C177
Skeletal	E D S N G C I N Y E A F V
Smooth	E D S N G C I N Y E E L V
Scallop	E D L E G N V K Y E D F V

[†]Xu and Root (1998).
[¶]Xiao et al. (1998).
[§]Smyczynski and Kasprzak (1997).
[‡]G21 is used as an indicator of the RLC position, because it is the residue on the ELC nearest to the RLC, and the RLC is not present in the atomic model of smooth muscle S1.

steps. ATP binding is important to prevent ADP rebinding, while phosphate release and the transition from a weak-to-strong binding state keeps the weak binding S1 from dissociating prematurely from actin. The lever arm model requires that the myosin head be firmly attached to actin when the lever arm swings during force generation, yet the ADP-Pi state and the transition state analogs ADP-BeF_x, ADP-AlF_4, and ADP-vanadate all induce weak actin binding conformations in S1. It has been suggested that ADP-AlF_4 and ADP-vanadate induce the pre-powerstroke state, but the pre-powerstroke state must bind strongly to actin for force to be produced, so an additional transition is necessary that involves actin binding before the powerstroke. It is possible that this transition is important for selecting a pre-powerstroke state cross-bridge based on the position of the lever arm or the angle of cross-bridge attachment, or both. If such a "conformational selection" occurs at this point, then the lever arm must not completely pre-cock during ATP hydrolysis of the detached myosin head. It is possible that a variety of lever arm positions might exist at any given time, but only the appropriately oriented lever arm will produce a conformation that allows the catalytic domain to bind to actin. A signaling mechanism for such a conformational selection is evident in that the lever arm position is linked to the conformation of the SH1–SH2 region and ultimately to the nucleotide cleft and the actin binding site.

Different positions of the RLC relative to actin in weak versus strong actin binding states

Beyond the difficulty in correlating bound nucleotides with crystallographic structures, other lines of evidence suggest that several conformations of myosin and its lever arm may exist in the weakly bound state. Electron microscopy detects a wide variety of cross-bridge attachment angles to actin and lever arm positions on myosin (Craig et al., 1985; Applegate and Flicker, 1987; Pollard et al., 1993; Schmitz et al., 1997). Resonance energy transfer data have not been consistently successful in detecting a pre-cocked state of the lever arm using nucleotide transition state analogs (Smyczynski and Kasprzak, 1997; Xu and Root, 1998; Table 4). EPR data suggest that relatively large distributions of probe orientations exist in the weak binding state. Fluorescence polarization measurements suggest a similar broad distribution of probe orientations. If so many different conformations exist, how can one be certain that an individual crystallographic structure represents the pre-powerstroke state? The binding to actin might be necessary to select a pre-powerstroke state conformation that leads to force generation.

The RET data between Cys-374 and the RLC are consistent with a relatively close average position of the RLC to actin. If the myosin catalytic domain had a single fixed orientation on actin and the lever arm adopted a combination of conformations corresponding to crystallographic

states I-III during binding to actin, the average RET distance between Cys-374 and the RLC would be predicted to be relatively small, on the average. The high degree of bending in states II and III would require the RLC to closely approach the actin filament. This type of scenario is quite consistent with the efficiencies of RET that are observed even in the strong binding state. In the weak binding state, the RLC moves very close to the Cys-374, on the average. Such a change would be consistent with differences in the lever arm position, the angle of S1 attachment to actin, or a repositioning of the C-terminus of actin. The efficiency of RET nearly doubles between strong binding and weak binding states, and some variations between the nucleotide analogs that induce weak binding states are observed (Table 3). Therefore, the form of the nucleotide bound does influence the conformation of the catalytic domain, but it does not appear to induce a full pre-cocking of the myosin until weak binding to actin.

This apparent conformational selection may reflect a distinct position of the lever arm relative to the catalytic domain that signals through the SH1-SH2 region that the myosin is ready to proceed through the powerstroke. It also provides a means for synchronization of myosin heads during muscle contraction by a communication through the thick filament by which myosin heads are linked. If one myosin head is in the process of making a productive weak binding interaction with actin, a motion of the thick filament will alter the position of the lever arm on that aspiring cross-bridge and prevent its initiation into the powerstroke event. In this way, cross-bridges may be recruited until the thick filament moves, at which point the recruitment process begins again. A thick filament that is impeded in its motion will recruit more cross-bridges and produce more ATPase activity, consistent with previous observations on chemically modified thick filaments that translocated actin at reduced rates during in vitro motility assays and yet accelerated actin-activated ATPase rates (Root and Reisler, 1992). The subsequent force generating conformational changes could involve rotations of the catalytic domain relative to the lever arm or actin, and/or elastic elements in the myosin S2 or actin. With the atomic models of S1 hypothetically fitting into the ATPase cycle, a working model for the role of conformational selection in the cyclic interaction of myosin with actin during one ATP turnover is illustrated in Fig. 6.

The data reported here support the view that the lever arm position does not completely pre-cock upon ATP hydrolysis in solution with a magnitude equal to the 12 nm or greater powerstroke length that has been reported frequently in the literature. We suggest that the full pre-cocking of the myosin head requires structural changes at the actomyosin interface during weak binding to actin. Further evidence is presented that during the weak actin binding the RLC is substantially closer to Cys-374 on actin than during strong

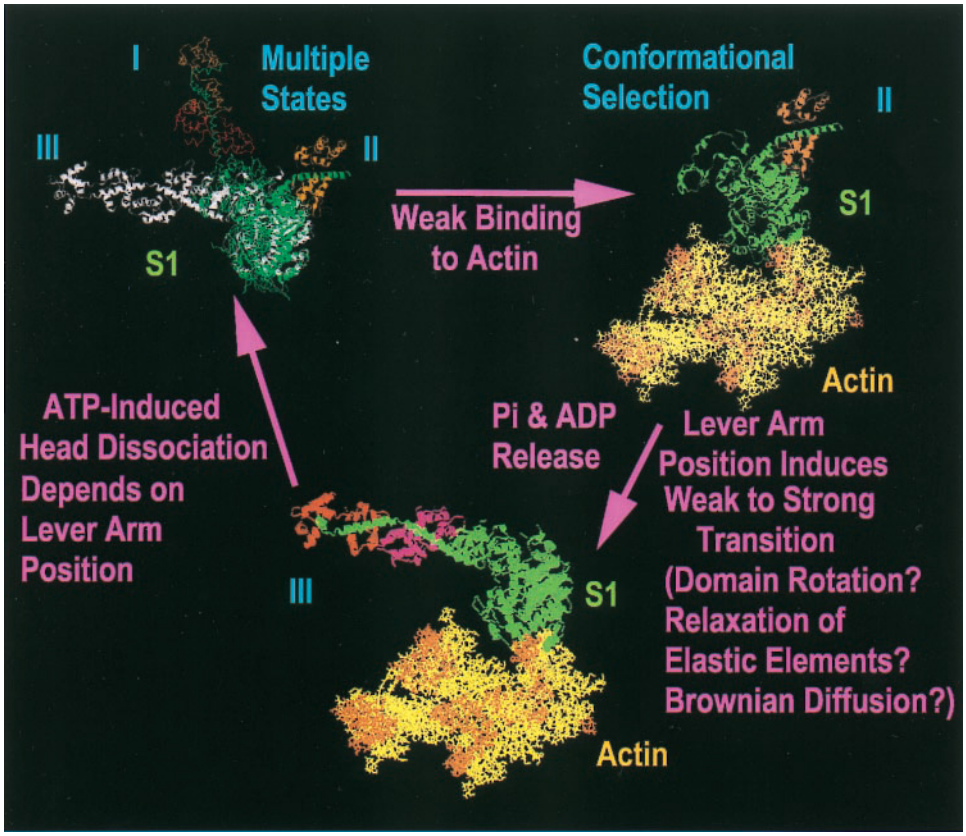

FIGURE 6 A working model for the role of conformational selection in the cyclic interaction of myosin with actin. Atomic models of S1 representing three distinct structural states as described in Table 4 are presented as they hypothetically fit into the ATPase cycle and cyclic interactions with actin. It is suggested that the orientation of the lever arm is sensed by conformational changes in the SH1 and SH2 region of myosin that regulate phosphate release, nucleotide binding, and actomyosin interactions. In this manner it is possible for the ATPase cycle to proceed when the myosin head is in an optimal conformation to initiate a powerstroke. It is conceivable that the directionality of molecular motors is determined by this type of mechanism.

binding, and transition states can be detected upon the addition of nucleotide analogs. These data provide evidence for participation of the actomyosin interface in a conformational selection process leading to the powerstroke that is not currently described in some versions of the swinging lever arm hypothesis.

We thank Dr. Julian Borejdo for his comments on the manuscript.

This work was supported by National Institutes of Health Grant AR44737.

REFERENCES

Adhikari, B., K. Hideg, and P. G. Fajer. 1997. Independent mobility of catalytic and regulatory domains of myosin heads. *Proc. Natl. Acad. Sci. U.S.A.* 94:9643–9647.

Allen, S. C. T., N. Ling, M. Irving, and Y. Goldman. 1996. Orientation changes in myosin regulatory light chains following photorelease of ATP in skinned muscle fibers. *Biophys. J.* 70:1847–1862.

Andreeva, A. L., O. A. Andreev, and J. Borejdo. 1993. Structure of the 265 kDa complex formed upon EDC cross-linking of subfragment1 to F-actin. *Biochemistry.* 32:13956–13960.

Applegate, D., and P. Flicker. 1987. New states of actomyosin. *J. Biol. Chem.* 262:6856–6863.

Bader, D., T. Masaki, and D. A. Fischman. 1982. Immunochemical analysis of myosin heavy chain during avian myogenesis in vivo and in vitro. *J. Cell Biol.* 95:763–770.

Baker, J. E., I. Brust-Mascher, S. Ramachandran, L. E. Laconte, and D. D. Thomas. 1998. A large and distinct rotation of the myosin light chain domain occurs upon muscle contraction. *Proc. Natl. Acad. Sci. U.S.A.* 95:2944–2949.

Berger, C. L., and D. D. Thomas. 1993. Rotation dynamics of actin-bound intermediates of the myosin adenosine triphosphate cycle in myofibrils. *Biophys. J.* 67:250–261.

Burghardt, T. P., S. P. Garamszegi, and K. Ajtai. 1997. Probes bound to myosin Cys-707 rotate during length transients in contraction. *Proc. Natl. Acad. Sci. U.S.A.* 94:9631–9636.

Burke, M., and E. Reisler. 1977. Effect of nucleotide binding on the proximity of the essential sulfhydryl groups of myosin. Chemical probing of movement of residues during conformational transitions. *Biochemistry.* 16:5559–5563.

Cooke, R. 1997. Actomyosin interaction in striated muscle. *Physiol. Rev.* 77:671–697.

Cooper, J. A., S. B. Walker, and T. D. Pollard. 1983. Pyrene actin: documentation of the validity of a sensitive assay for actin polymerization. *J. Muscle Res. Cell Motil.* 4:253–262.

Craig, R., L. E. Greene, and E. Eisenberg. 1985. Structure of the actin-myosin complex in the presence of ATP. *Proc. Natl. Acad. Sci. U.S.A.* 82:3247–3251.

Dominguez, R., Y. Freyzon, K. M. Trybus, and C. Cohen. 1998. Crystal structure of a vertebrate smooth muscle myosin motor domain and its complex with the essential light chain: visualization of the pre-power stroke state. *Cell.* 94:559–571.

Finer, J. T., R. M. Simmons, and J. A. Spudich. 1994. Single myosin molecule mechanics: piconewton forces and nanometre steps. *Nature.* 368:113–119.

Fisher, A. J., C. A. Smith, J. B. Thoden, R. Smith, K. Sutoh, H. M. Holden, and I. Rayment. 1995. X-ray structures of the myosin motor domain of *Dictyostelium discoideum* complexed with MgADP · BeF_x and MgADP · AlF_4^-. *Biochemistry.* 34:8960–8972.

Funatsu, T., Y. Harada, M. Tokunaga, K. Saito, and T. Yanagida. 1995. Imaging of single fluorescent molecules and individual ATP turnovers by single myosin molecule in aqueous solution. *Nature.* 374:555–559.

Getz, E. B., R. Cooke, and P. R. Selvin. 1998. Luminescence resonance energy transfer measurement in myosin. *Biophys. J.* 74:2451–2458.

Godfrey, J. E., and W. F. Harrington. 1970. Self-association in the myosin system at high ionic strength. I. Sensitivity of the interaction to pH and ionic environment. *Biochemistry.* 9:886–895.

Goldman, Y. E. 1998. Wag the tail: structural dynamics of actomyosin. *Cell.* 93:1–4.

Higuchi, H., and Y. E. Goldman. 1991. Sliding distance between actin and myosin filaments per ATP molecule hydrolyzed in skinned muscle fibres. *Nature.* 352:352–354.

Holmes, K. C. 1997. The swinging lever-arm hypothesis of muscle contraction. *Curr. Biol.* 7:R112–R118.

Houdusse, A., V. N. Kalabokis, D. Himmel, A. G. Szent-Gyorgyi, and C. Cohen. 1999. Atomic structure of scallop myosin subfragment S1 complexed with MgADP: a novel conformation of the myosin head. *Cell.* 97:459–470.

Huxley, H. E., and A. R. Faruqi. 1983. Time-resolved x-ray diffraction studies on the vertebrate striated muscle. *Annu. Rev. Biophys. Bioeng.* 12:381–417.

Huxley, H. E., and M. Kress. 1985. Crossbridge behavior during muscle contraction. *J. Muscle Res. Cell Motil.* 6:153–161.

Huxley, A. F., and R. M. Simmons. 1971. Proposed mechanism of force generation in striated muscle. *Nature.* 233:533–538.

Ishijima, A., Y. Harada, H. Kojima, T. Funatsu, H. Higuchi, and T. Yanagida. 1994. Single-molecule analysis of the actomyosin motor using nano-manipulation. *Biochem. Biophys. Res. Commun.* 199: 1057–1063.

Jontes, J. D., and R. A. Milligan. 1997. Brush border myosin-1 structure and ADP-dependent conformational changes revealed by cryoelectron microscopy and image analysis. *J. Cell Biol.* 139:683–693.

Kabsch, W., H. G. Mannherz, D. Suck, E. F. Pai, and K. C. Holmes. 1990. Atomic structure of actin DNAse I complex. *Nature.* 347:37–44.

Kron, S. J., Y. Y. Toyoshima, T. Q. P. Uyeda, and J. A. Spudich. 1991. Assays for actin sliding movement over myosin-coated surface. *Methods Enzymol.* 196:399–416.

Lymn, R., and E. W. Taylor. 1971. Mechanism of adenosine triphosphate hydrolysis by actomyosin. *Biochemistry.* 10:4617–4624.

Phan, B. C., L. D. Faller, and E. Reisler. 1993. Kinetic and equilibrium analysis of the interactions of actomyosin subfragment-1 · ADP with beryllium fluoride. *Biochemistry.* 32:7712–7719.

Piazzesi, G., M. Reconditi, J. Dobbie, M. Linari, P. Boesecke, O. Diat, M. Irving, and V. Lombardi. 1999. Changes in the conformation of myosin heads during the development of isometric contraction and rapid shortening in single frog muscle fibres. *J. Physiol.* 514:305–312.

Pollard, T. D., D. Bhandari, P. Maupin, D. Wachsstock, A. G. Weeds, and H. G. Zot. 1993. Direct visualization by electron microscopy of the weakly bound intermediates in the actomyosin adenosine triphosphatase cycles. *Biophys. J.* 64:454–471.

Rayment, I., H. M. Holden, M. Whittaker, C. B. Yohn, M. Lorenz, K. C. Holmes, and R. A. Milligan. 1993. Structure of the actin-myosin complex and its implications for muscle contraction. *Science.* 261:58–65.

Root, D. D. 1997. In situ molecular association of dystrophin with actin revealed by sensitized emission immuno-resonance energy transfer. *Proc. Natl. Acad. Sci. U.S.A.* 94:5685–5690.

Root, D. D., and E. Reisler. 1992. Cooperativity of thiol-modified myosin filaments: ATPase and motility assays of myosin function. *Biophys. J.* 63:730–740.

Root, D. D., X. Shangguan, J. Xu, and M. McAllister. 1999. Determination of fluorescent probe orientations on biomolecules by conformational searching: algorithm testing and applications to the atomic model of myosin. *J. Struct. Biol.* 127:22–34.

Root, D. D., and K. Wang. 1994. Calmodulin-sensitive interaction of human nebulin in fragments with actin and myosin. *Biochemistry.* 33: 12581–12591.

Schmitz, H., M. C. Reedy, M. K. Reedy, R. T. Tregear, and K. A. Taylor. 1997. Tomographic three-dimensional reconstruction of insect flight muscle partially relaxed by AMPPNP and ethylene glycol. *J. Cell Biol.* 139:695–707.

Selvin, P. R., and J. E. Hearst. 1994. Luminescence energy transfer using a terbium chelate: improvements on fluorescence energy transfer. *Proc. Natl. Acad. Sci. U.S.A.* 91:10024–10028.

Smyczynski, C., and A. A. Kasprzak. 1997. Effect of nucleotide and actin on the orientation of light chain-binding domain in myosin subfragment 1. *Biochemistry.* 36:13201–13213.

Spudich, J. A., and S. Watt. 1971. The regulation of rabbit skeletal muscle contraction. I. Biochemical studies of the interaction of the tropomyosin-troponin complex with actin and the proteolytic fragments of myosin. *J. Biol. Chem.* 246:4866–4871.

Thomas, D. D., S. Ramachandran, O. Roopnarine, D. W. Hayden, and E. M. Ostap. 1995. The mechanism of force generation in myosin: a disorder-to-order transition, coupled to internal structural changes. *Biophys. J.* 68:135s–141s.

Uyeda, T. Q., P. D. Abramson, and J. A. Spudich. 1996. The neck region of the myosin motor domain acts as a lever arm to generate movement. *Proc. Natl. Acad. Sci. U.S.A.* 93:4459–4464.

Wagner, P. D. 1982. Preparation and fractionation of myosin light chains and exchange of the essential light chains. *Methods Enzymol.* 85:72–81.

Weeds, A. G., and B. Pope. 1977. Studies on the chymotryptic digestion of myosin: effects of divalent cations on proteolytic susceptibility. *J. Mol. Biol.* 111:129–157.

Wells, J. A., and R. C. Yount. 1979. Active site trapping of nucleotides by crosslinking two sulfhydryls in myosin subfragment 1. *Proc. Natl. Acad. Sci. U.S.A.* 76:4966–4970.

Werber, M. M., Y. M. Peyser, and E. Reisler. 1997. Nucleotide and actin binding properties of isolated motor domain from Dictyostelium discoideum myosin. *J. Muscle Res. Cell Motil.* 18:563–571.

Whittaker, M., E. M. Wilson-Kulabek, J. E. Smith, L. Faust, R. A. Milligan, and H. L. Sweeney. 1995. A 35-Å movement of smooth muscle myosin on ADP release. *Nature.* 387:748–751.

Wolff-Long, V. L., T. Tao, and S. Lowey. 1995. Proximity relationships between engineered cysteine residues in chicken skeletal myosin regulatory light chain. *J. Biol. Chem.* 270:31111–31118.

Xiao, M., H. Li, G. E. Snyder, R. Cooke, R. G. Yount, and P. R. Selvin. 1998. Conformational changes between the active-site and regulatory light chain of myosin as determined by luminescence resonance energy transfer: the effect of nucleotides and actin. *Proc. Natl. Acad. Sci. U.S.A.* 95:15309–15314.

Xu, J., and D. D. Root. 1998. Domain motion between the regulatory light chain and the nucleotide site in skeletal myosin. *J. Struct. Biol.* 123: 150–161.